Pak. J. Bot., 58(5): 1163-1175, May 2026.

ARTICLE | DOI: http://dx.doi.org/10.30848/PJB2026-5(18)

NETWORK PHARMACOLOGY AND EXPERIMENTAL EVALUATION OF SINGHAR *CITRUS LIMON* PEEL ESSENTIAL OIL FOR BIOACTIVE AND ANTIBIOFILM PROPERTIES

ASMA AYAZ[1†], ADNAN AMIN[2†], SAJID ALI[3†], WAJID ZAMAN[2†], MINJUN LIANG[1], YAODONG GU[1*] AND YUN SEOK HEO[4*]

[1]Faculty of Sports Science, Ningbo University, Ningbo, 315211, China
[2]Department of Life Sciences, Yeungnam University, Gyeongsan 38541, Republic of Korea
[3]Department of Horticulture and Life Science, Yeungnam University, Gyeongsan 38541, Republic of Korea
[4]Department of Mechanical & System Design Engineering, Hongik University, 94 Wausan-ro, Mapo-gu, Seoul, 04066, Republic of Korea

*Corresponding author's email: guyaodong@nbu.edu.cn /yunsheo@hongik.ac.kr
†Contributed equally to this work

Abstract

Citrus limon peel is a rich source of bioactive monoterpenes that exhibit potential antimicrobial and antioxidant activities. This study aimed to comprehensively characterize the phytochemical composition and biofunctional mechanisms of the indigenous Singhar seedless variety *C. limon* peel essential oil (EO) by using integrated experimental and *in silico* approaches. The EO was extracted by hydro-distillation and analyzed via GC–MS**.** Network pharmacology and molecular docking were employed to elucidate molecular targets and pathways underlying the EO's antibacterial mechanisms. Antioxidant activity was evaluated using DPPH, FRAP, and H_2O_2 assays, while antibacterial and antibiofilm assays were performed against *Staphylococcus aureus* strains., revealed 21 compounds, including limonene (61.2%), *p*-menth-8-en-ol acetate (14.1%), α-terpinene (10.2%), and linalyl anthranilate (9.2%). Network pharmacology identified 71 overlapping targets, including STAT3, MAPK14, and MAPK1, which are GC–MS enriched in MAPK, IL-17, and VEGF signaling pathways. Docking simulations revealed favorable binding energies (−4.6 to −6.5 kcal/mol), suggesting that EO compounds can disrupt microbial and inflammatory signaling cascades. During experimental validation, the EO demonstrated potent antioxidant activity in a concentration-dependent manner (IC_{50} = 12.4 µg/mL) and exhibited notable antibacterial efficacy with MIC values ranging from 1.3–21.3 µg/mL, particularly against *S. aureus* ST-2. Biofilm inhibition reached 77.4% at 2% (v/v), and time-kill kinetics confirmed sustained activity up to 18 h. It was concluded that Singhar C. limon peel EO exerts its bioactivity through multitarget mechanisms, including antibacterial, antibiofilm, and oxidative stress modulation, thus substantiating its potential application as a natural therapeutic agent for managing *S. aureus* pneumonia infections. Given its food-grade origin, this essential oil also shows strong potential as a natural preservative and antioxidant ingredient for improving food safety and shelf-life.

Key words: *Citrus limon*; Essential oil; GC–MS; Antioxidant; Antibacterial; Antibiofilm; Network pharmacology; Molecular docking

Introduction

Essential oils (EOs) are volatile, naturally occurring compounds produced by plants as secondary metabolites, commonly serving biological functions such as defense against pathogens, herbivores, and environmental stressors (Al-Khayri *et al*., 2023). In recent decades, they have attracted significant scientific interest due to their diverse biological activities, including antimicrobial, antioxidant, anti-inflammatory, antiviral, and anticancer properties (Sharifi-Rad *et al*., 2017). In contrast to conventional synthetic pharmaceuticals, essential oils interact with multiple targets simultaneously, thereby reducing the likelihood of resistance development (Tullio, Roana, Cavallo, & Mandras, 2023). Their intricate chemical composition—typically comprising monoterpenes, sesquiterpenes, aldehydes, ketones, esters, and phenolic compounds—confers significant pharmacological potential (de Sousa *et al*., 2023). These compounds can penetrate bacterial membranes, modify cell permeability, impair enzymatic activity, and interfere with quorum sensing and other intercellular signaling pathways, ultimately hindering bacterial colonization and biofilm formation. The extensive scope of this activity, along with their natural origin and biocompatibility, has established essential oils as viable candidates for the development of novel antibacterial and antibiofilm agents (Tang *et al*., 2020).

The biological efficacy of an essential oil mostly depends on its principal components and their synergistic interactions. Compounds such as limonene, citral, linalool, and β-pinene are often recognized as the primary bioactive agents responsible for antibacterial and antibiofilm properties (Noumi *et al*., 2023). Limonene, a dominant monoterpene in citrus essential oils, has demonstrated the ability to disturb lipid membranes, inhibit bacterial adhesion, and modify intracellular signaling pathways that govern biofilm development. These chemical compounds not only affect bacterial cell walls and membranes but also disrupt the regulatory networks associated with quorum sensing, a critical mechanism that regulates biofilm development and the production of virulence factors (Subramenium, Vijayakumar, & Pandian, 2015). Comprehending these mechanisms is essential for developing innovative

Received: 18-06-2025 | Revised: 03-12-2025 | Accepted: 10-12-2025 | Online: 02-02-2026

antibiofilm approaches that are both efficacious and safe for clinical and industrial applications (Namivandi-Zangeneh, Yang, Xu, Wong, & Boyer, 2019).

Bacterial biofilms are highly organized, sessile communities encased in a self-generated extracellular polymeric matrix comprised of polysaccharides, proteins, and nucleic acids (Xinyu Wang, Liu, Yu, Li, & Zhou, 2023). This structure provides exceptional protection against adverse conditions, antimicrobial substances, and host immune responses. Up to 80% of persistent and recurring human infections, such as those brought on by *Klebsiella pneumoniae, Pseudomonas aeruginosa, Staphylococcus aureus*, and *Escherichia coli*, are thought to be biofilm-associated (Guerra *et al*., 2022). Among these, methicillin-resistant Staphylococcus aureus (MRSA) represents a major clinical challenge in pulmonary infections, where these bacteria form biofilms on mucosal surfaces and on indwelling respiratory devices such as endotracheal tubes, facilitating persistent colonization, immune evasion, and chronic disease (Pal, Rebuma, Regassa, & Zende, 2024). These biofilms hinder antibiotic diffusion and protect resident bacteria from phagocytic clearance, allowing MRSA to thrive in the hostile pulmonary environment. In pneumonia, MRSA biofilms exacerbate lung damage by secreting cytotoxic factors, such as alpha-hemolysin (Pickens & Wunderink), which compromise epithelial integrity and trigger robust but ineffective inflammatory responses, leading to alveolar injury, impaired gas exchange, and increased mortality.

Citrus limon (lemon), belonging to the Rutaceae family, is among the most commonly cultivated citrus species in tropical and subtropical areas, esteemed for its nutritive, aromatic, and medicinal significance. The essential oil, predominantly extracted from the fruit peel, is rich in monoterpenes including limonene, γ-terpinene, β-pinene, and citral (Paw, Begum, Gogoi, Pandey, & Lal, 2020). Many research studies have highlighted the antibacterial, antioxidant, and anti-inflammatory effects of *C. limon* essential oil; however, few have examined its antibiofilm potential and the mechanisms of action involved (Kačániová *et al*., 2024). The composition and efficacy of lemon essential oil vary considerably depending on factors such as genetic variety, geographical origin, soil composition, and environmental conditions. Therefore, the investigation of indigenous variation offers a unique opportunity to identify novel chemotypes with enhanced pharmacological properties and potential industrial significance (Gölükcü *et al*., 2024).

In this regard, the seedless variety "Singhar," cultivated in the Dera Ismail Khan region of Pakistan, is a compelling subject for investigation. This indigenous variety is renowned for its strong aroma, thin peel, and high essential-oil yield, which reflect a unique phytochemical profile. Despite its agricultural and commercial importance, the "Singhar" variety is underexplored in the scientific literature, and a thorough assessment of its antibiofilm efficacy has not yet been conducted. Characterizing its essential oil composition and evaluating its potential to inhibit bacterial biofilms could enhance natural-product-based therapeutics and contribute to the valorization of indigenous citrus germplasm within Pakistan's agro-industrial sector. Beyond its traditional medicinal uses, *C. limon* essential oil is of significant importance in the food and beverage industry. Limonene and other monoterpenes present in citrus peel are classified as Generally Recognized as Safe (GRAS) by the U.S. FDA, enabling their incorporation as natural flavoring agents, antioxidants, and antimicrobial preservatives in food products. Essential oils from citrus have been increasingly explored as alternatives to synthetic preservatives due to their ability to inhibit the growth of foodborne pathogens, suppress biofilm formation on food-contact surfaces, and delay lipid oxidation. Therefore, evaluating the bioactivity of *C. limon* essential oil is not only relevant for therapeutic purposes but also highly important for food quality, safety, and nutraceutical development. Therefore, this study examines the antibiofilm efficacy of indigenous *C. limon* "Singhar" essential oil through an integrated network pharmacology and in vitro antioxidant, antimicrobial, and antibiofilm models against methicillin-resistant *Staphylococcus aureu*s.

Materials and Methods

Essential oil extraction: The *Citrus limon* was freshly obtained from Singhar village, D.I. Khan, Pakistan (with consent), and the specimens were authenticated. Fresh peel was removed, pulverized, and macerated overnight. The essential oil (EO) was extracted in the lab by using the Clevenger apparatus (hydrodistillation). Collected EO dehydrated with sodium sulfate and stored (2-4°C) till onward use.

Growth media and bacterial strains: The clinical strains of *Staphylococcus aureus (*ST_1 to ST-4*)* were provided by Dr. Momin Khan, Department of Microbiology, Khyber Medical University, Peshawar, Pakistan, whereas the standard strain used was BAA1707. The bacterial growth media, including nutrient agar, nutrient broth, and Tryptic Soy Broth (TSB), were procured from HiMedia (India). Standard antibiotics, ciprofloxacin, DPPH, H2O2, and TPTZ, were purchased from Oxoid (UK).

Analytical procedure

GC-MS analysis: The GCMS analysis was performed by the previously described method. Briefly, the GC machine (Shimadzu GC-2010, Japan) was equipped with an autosampler (AOC-20i) and a DB-5 MS capillary column (30 m × 0.25 mm i.d., 0.25 µm film thickness). For loading the sample, an aliquot of essential oil (0.5 µL) was used. GC-MS component analysis and identification were accomplished on a GC-MS-QP 2010 Plus (Shimadzu, Japan) system operating in EI mode (electron ionization mode) at 70 eV. Mass units were monitored from 35 to 500 AMU. The mass spectral library (NIST) and compound mix were used for compound identification.

Computational assays

Network pharmacology

Screening of targets of isolated compounds: The molecular structures (2D) and SMILES notations for major compounds, including limonene, β-pinene, linalyl anthranilate, Myrcene, p-menth-8-en-ol, acetate, and terpineol, were downloaded from PubChem. Compound-target predictions were executed by using Swiss-Target-

Prediction. Targets with prediction scores ≥ 90% were considered significant and used for further analysis (Xiaowan Wang *et al*., 2025).

Potential Targets for *Staphylococcus aureus pneumonia*: The disease-related targets, i.e., "*Staphylococcus aureus pneumonia,*" were obtained from GeneCards by using the same search keyword. Targets with GeneCards relevance scores ≥ 0.5 were designated as the screening standards. Further, the overlapping genes amongst the compounds and target gene sets were acknowledged using a Venn diagram tool (Venny 2.03). These crossing genes were considered as potential therapeutic targets for *S. pneumonia*.

Protein–protein interaction network construction: The standard targets were further analyzed using the STRING database to construct a protein-protein interaction (PPI) network, using an interaction score threshold of > 0.7. Network analysis and final visualization were performed using Cytoscape 3.9.0.

Enrichment analysis: The GO (Gene Ontology) and KEGG (Kyoto Encyclopedia of Genes and Genomes) analyses were conducted to explore central molecular mechanisms across MF (molecular functions), BP (biological processes), and CC (cellular components). These studies were performed using the DAVID database (with Homo sapiens filter*)*. The top 10 most significant "enriched pathways" were finally selected for visualization and further processing. Besides, the GO and KEGG results were investigated and visualized using an online bioinformatics platform (http://www.bioinformatics. com.cn/) and the ShinyGO 0.82 tool (https://bioinformatics. sdstate.edu/go/16).

Construction of the component-target-pathway network: A "component-target-pathway" regulatory network was constructed by integrating the common targets identified from compound-disease relationships with the top predicted pathways. The network was generated and analyzed in Cytoscape 3.9.0, and the hub gene was identified.

Molecular docking: From network pharmacology analysis, 10 hub genes were identified, and among them, the top 3 hub genes, including STAT3 (PDB: 1BG), MAPK14 PDB ID: 7BDO), and MAPK1 (PDB: ID 1PME), were used for molecular docking. using Lamarckian Genetic Algorithm in AutoDock v4.2 (Trott & Olson, 2010). All generated poses were evaluated based on their binding free energy and RMSD values using the following formula:

$$RMSD = \sqrt{\frac{1}{N}\Sigma_{\{i=1\}}^{\{N\}}\left[(x_i - x_{\{i,ref\}})^2 + (y_i - y_{\{i,ref\}})^2 + (z_i - z_{\{i,ref\}})^2\right]}$$

The xi, ref, yi, ref, zi, ref correspond to the reference pose (e.g., the lowest-energy conformation or crystallographic pose) and N is the number of atoms in the ligand; xi, yi, zi are the coordinates of atom i in the docked pose. RMSD values ≤ 2.0 Å indicate stable binding poses. The visualization was performed by using Accelrys Discovery Studio Visualizer 2.0 (Accelrys Software Inc., 2012).

***In vitro* Biological Activities**

Antioxidant assay: Oxidative stress inhibition was assessed using the following assays:

2.5.1.1 DPPH radical scavenging assay: DPPH scavenging activity was assessed using the established protocol 18. Briefly, a fresh DPPH solution in methanol (0.1 mM; 50 µL) was prepared in a 96-well microplate and mixed with the sample or standard (50 µL; 200–1.56 µg/mL). The mixture was then incubated in a dark cabinet for 35 minutes. Finally, absorbance was recorded at 517 nm using a microplate reader. The Ascorbic acid was the standard. Percentage (%) inhibition was calculated as follows:

$$\%\ Inhbition = \left[1 - \frac{Aa}{Ab}\right] x\ 100$$

where *Aa* represents the sample absorbance, and *A*b indicates the control absorbance. IC_{50} values for the tested samples were calculated from linear plots.

Ferrous-reducing antioxidant assay: The ferrous-reducing antioxidant power (FRAP) was determined using an established protocol (Azad & Chhatria, 2025). Briefly, a fresh FRAP reagent was prepared by mixing TPTZ solution (10 mL; 10 mM), acetate buffer (100 mL; 300 mM), and FeCl3·6H2O (10 mL; 20 mM). Test samples (150 µL; 25 µg) were added to FRAP reagent (2850 µL), and the mixture was incubated in the dark for at least 35 minutes. Absorbance was finally measured at 593 nm. A $FeSO_4$ calibration curve (0–100 µg/mL) was generated, and the results were expressed as mg Fe+ equivalents.

Hydrogen peroxide scavenging activity: The scavenging activity against hydrogen peroxide (H_2O_2) was assessed using a standard procedure (Azad & Chhatria, 2025). The EO or standard drug (ascorbic acid) or Blank (DMSO, >5%) solutions (400 µL at various concentrations) were combined with H2O2 solution (600 µL, 2 mM), followed by gentle vortexing for 1 min and incubation at room temperature for 15 min. The absorbance of the final solution was recorded at 230 nm using a UV spectrophotometer. Finally, the percentage % of inhibition was calculated as;

$$\%\ Inhbition = \left[1 - \frac{Aa}{Ab}\right] x\ 100$$

where *Aa* represents the sample absorbance, and ***A***b represents the control absorbance.

Antimicrobial activity

Inhibition zones and MICs: The antibacterial activity of essential oils was determined using 96-well microplates (MIC method) as described previously(Amanullah et al., 2025). In brief, the test samples were inoculated with 50 µL of an overnight culture of S. aureus (1.5×10^7 CFU/mL), and then 50 µL of the test samples (various dilutions) were added to each well. The microplates were incubated at 37°C for an additional 24 hours. Afterwards, an aliquot of

40 µL of resazurin solution (0.015%) was added to each well, and the plates were placed at 37°C for an extra 60 minutes. All colorimetric analyses were performed using a 96-well microplate reader.

Antibiofilm activity and time kinetics: Antibiofilm assay was achieved by using microwell plates (12-wells), using a modified protocol (Amanullah *et al*., 2025). Initially, the bacterial strains were inoculated into 280 µL of Tryptic Soy Broth (TSB) to achieve an initial optical density of 0.5 at 600 nm. The bacterial cultures were then incubated for 24 hours. Later, 100 µL of the EO was added to each well, and the incubation continued at 37°C for an additional 24 hours. The bacterial growth was measured at 592 nm. Later, the biofilms were stained (crystal violet), and for quantification, solubilization of stain was performed (with 95% ethanol). Finally, absorbance at 592 nm was measured. The percentage inhibition was calculated using the following formula;

$$\% \, Inhbition = \left[1 - \frac{Aa}{Ab}\right] x \, 100$$

The Aa is the absorbance of the sample, and Ab is the absorbance of the control.

Time-kill kinetics were performed as previously described. The bacterial suspensions in the test sample were incubated at 37°C, and 100 µL aliquots were collected at regular intervals up to 24 hours from each tube, inoculated onto agar plates, and the CFU were counted; the results were recorded.

Statistical analysis

The mean of three experimental readings with SD (standard deviation) was used to demonstrate experimental results. A statistically significant difference was observed ($p<0.05$); SPSS version 24.0 was used for statistical analysis. Post hoc analysis using Tukey's HSD test was used where required.

Results

Plant material and EO isolation: The collected EO was initially transparent and turned to light yellow afterwards. The overall EO yield was 0.92%.

GC-MS analysis: A total of 21 compounds were identified in GC-MS analysis using a standard mix and the NIST library. Significantly high concentration of limonene (61.2%) was recorded, followed by p-menth-8-en-ol acetate (14.1%), α -terpinene (10.2), Linalyl anthranilate (9.2), Myrcene (6.4), and β-pinene (2.03%) (Table 1). A detailed overview of all compounds is presented in Table 1, Figs. 1-2.

Prediction of *Major components* and their antibacterial targets: From GCMS analysis, two major components from each plant, including Myrcene, p-menth-8-en-ol acetate, Limonene, Linalyl anthranilate, β-pinene, and α-Terpineol, were evaluated further for network pharmacology analysis. The Swiss target prediction revealed (after removal of duplicates) a total of 254 unique targets for these compounds. Similarly, the Genecards database was accessed for analysis of disease-related genes and the keyword "*Staphylococcus aureus* pneumoniae". This identified a total of 1943 antibacterial targets (after removing duplicates). Furthermore, common genes were identified using Venny (2.0), which yielded 71 overlapping targets between the two data sets (Fig. 3).

Table 1. GC-MS profile of *Citrus limon* peel essential oil.

S.No.	Name	R.Time	Conc %	KI*
1.	Myrcene	6.77	6.4	993
2.	α -terpinene	7.55	10.2	955
3.	p-menth-8-en-ol acetate	7.68	14.1	968
4.	Limonene	7.84	61.2	1348
5.	Linalyl anthranilate	8.74	9.2	1074
6.	o-Cymene	8.79	0.56	1081
7.	β-pinene	10.04	2.03	1204
8.	Linalool	10.11	0.14	1211
9.	p-menth-1-en-8-ol	10.18	2.3	1218
10.	Geraniol	10.20	2.04	1220
11.	Caryophyllene	10.22	0.24	1224
12.	Carveol	10.24	0.13	1226
13.	β-citral	10.82	0.07	1282
14.	α-citral	11.22	1.03	1322
15.	Citronellal	11.81	0.24	1471
16.	Camphor	12.16	0.04	1416
17.	Perillol	12.18	0.08	1481
18.	Decanal	13.68	0.36	1129
19.	α Terpineol	14.44	0.08	1644
20.	Neral	18.53	11.2	2053
21.	cis-α-Bergamotene	24.79	0.24	2679

*Kovats retention index

Table 2. Major outcomes of the PPI network.

S. No.	Parameter	Outcome
1.	Number of nodes	71
2.	Number of edges	110
3.	Average node degree	3.1
4.	Average local clustering coefficient	0.514
5.	PPI enrichment p-value	$< 10^{-16}$

Constructing the PPI network along with identifying the core targets: The protein-protein interactions (PPIs) were constructed using the STRING database (confidence score > 0.700) and a false discovery rate (FDR) of 5%. The network contained 110 nodes and 110 edges, with an average node degree of 3.1 and an average local clustering coefficient of 0.51 ($p<1.0 \times 10^{-16}$) (Table 2, Fig. 4). It was evident that the PPI network is incredibly interconnected and possesses a substantial functional relevance. The PPI network was further analyzed using Cytoscape software (version 3.10.1) (Fig. 4) to guide hub-gene identification and PPI analysis. The cytoHubba plugin in Cytoscape (Version 3.10.1) identified the top 10 hub genes using the degree method. The cytoNCA plugin was used to assess network topology, measuring degree, betweenness, and closeness centrality. The Merged network (including pathway) comprised 125 nodes and 245 edges. Hub-gene analysis using the cytoHubba tool revealed STAT3, MAPK14, MAPK1, ESR1, PTGS2, MAPK3, EGFR, MAPK8, PPARG, and PLA2G4A as key hub genes (Fig. 4). Similarly, the cytoNca was used to find out the degree of centrality and betweenness among network genes, which in fact exhibited a strong interaction among genes in the network (Table 3).

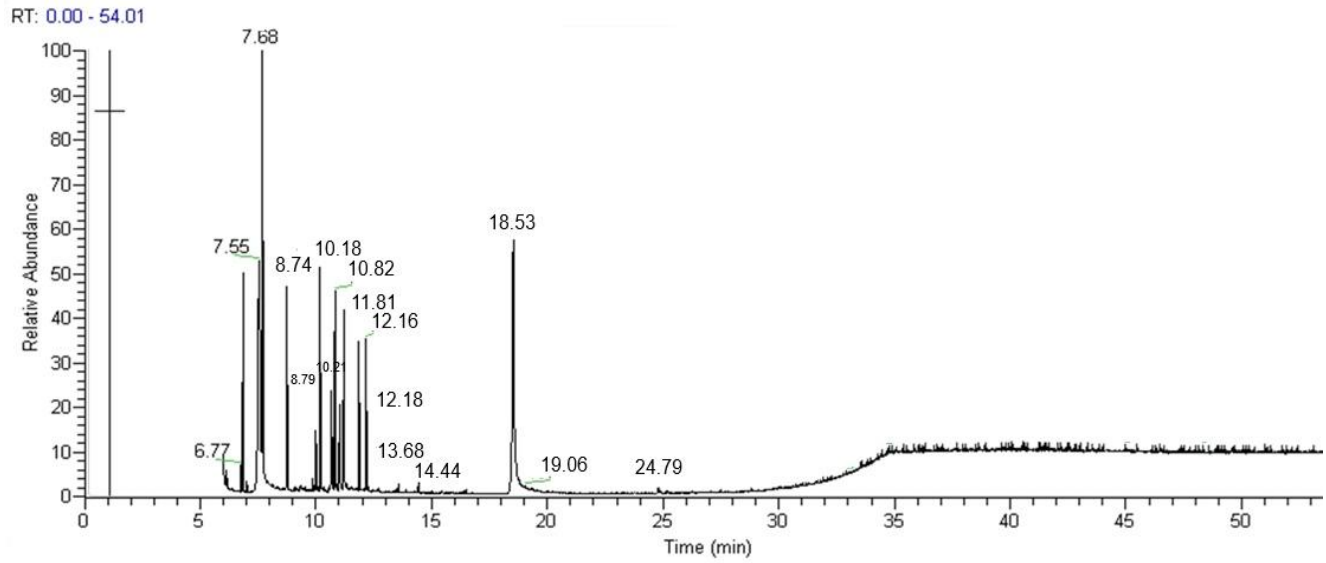

Fig. 1. GCMs analysis of Singhar *C. limon* essential oil.

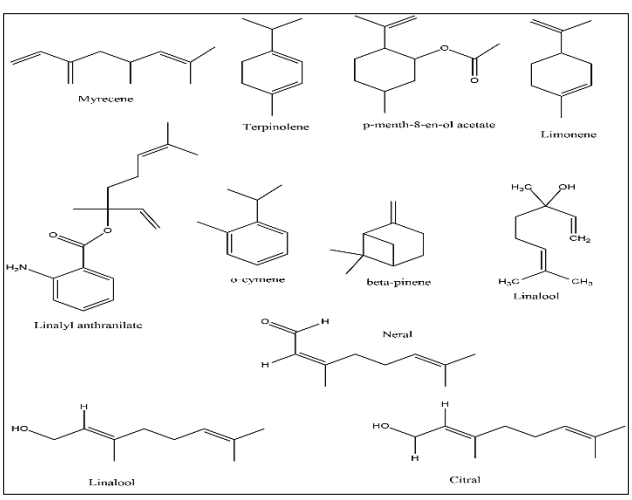

Fig. 2. Structure of Singhar *C. limon* essential oil major compounds.

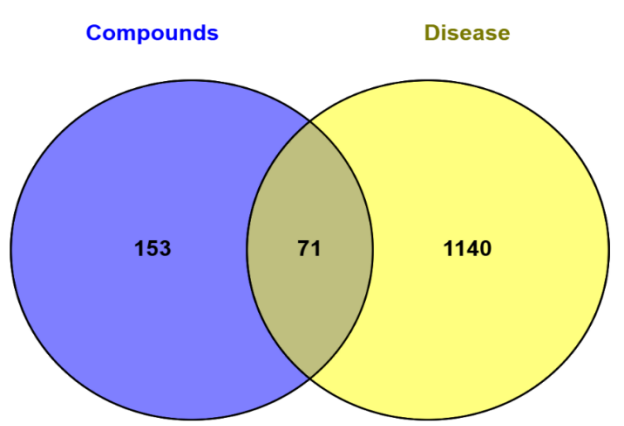

Fig. 3. Venn diagram showing common genes.

GO functional and KEGG pathway enrichment analysis: The GO Enrichment analysis was accomplished using the DAVID database (https://davidbioinformatics.nih.gov/summary.jsp). From there, KEGG, biological processes, cellular components, and molecular functions datasets were obtained and filtered by *P*-values (≤ 0.05), and the top 10 scores were selected for further analysis. GO enrichment analysis was accomplished using Open SRPlot (https://www.bioinformatics.com.cn/), and KEGG pathway analysis was performed using the ShinyGo tool (https://bioinformatics.sdstate.edu/go/). Results with $P < 0.05$ and enrichment factors > 1.5 were considered significant. GO enrichment revealed 184 Biological Processes (BP), 45 Cellular Components (CC), and 53 Molecular Functions (MF). Fig. 5 illustrates the top 10 terms in each category using visualized bar plots and circular plots (Fig. 5). Key BP included positive regulation of nitric-oxide synthase activity, phosphatidylcholine catabolic process, regulation of cardiac muscle cell contraction, positive regulation of triglyceride biosynthetic process, peptidyl-tyrosine autophosphorylation, etc., and MF heterocyclic compound binding, lipid binding, oxidoreductase activity, estrogen response element binding, sequence-specific DNA binding, etc.

Based on the same threshold (*p*-value < 0.05), the top 20 KEGG pathways were enriched and presented in a bubble chart (Fig. 5). Here, **Red** (FDR around 10) indicates the **most significant pathways**, with the smallest number of false discoveries. In contrast, the **Pink** (FDR around 9) is still substantial but may include a few more false discoveries. Based on these, the KEGG pathway analysis showed significant enrichment in pathways including the VEGF signaling pathway, IL-17 signaling pathway, TNF signaling pathway, and MAPK signaling pathway (Fig. 5).

Molecular docking investigations: Molecular docking of 2 major compounds of EO, including limonene and *p*-menth-8-en-ol-acetate, against different targets for *S. aureus* pneumonia was performed. The identified targets were obtained through network pharmacology (hub genes), including STAT3 (PDB ID 1BG1), MAPK14 (PDB ID 7BDO), and MAPK1 (PDB ID 1PME). In case of limonene, the interaction analysis with regulator gene 1BG1, the highest free energy was recorded in case of 7BDO (-5.8 ΔG (kJ mol^{-1}) and neighboring amino acids were Val30, Phe169, Tyr35, Leu108, Val38, Met109,

Ala51, Lys53, Thr106. Likewise, a strong interaction with high free energy (-5.8 ΔG (kJ mol^{-1}) was recorded. Here, the key participating amino acids included Leu103, Ile86, Cys166, Leu75, Lys54, Ala52, Val39, Ile84, Thr105, with no H-bonding interaction in all the targets (Table 4, Fig. 6).

In the case of p-menth-8-en-ol-acetate transcriptional regulator 1BG1, a significant H–bonding interaction with the target was recorded (**Asp 167)**. This interaction was supported by high free energy ((-6.4ΔG (kJ mol^{-1}) and neighboring amino acids were Cys166, Ile84, Ile31, Met108, Leu156, Ala52, Val 39, Leu107, Thr105, His106, Leu103, Lys54, Phe168, Leu75, Glu71. Likewise, a significant interaction was observed between 1PME (-5.8 ΔG (kJ mol–1)) and Arg335, which interacted via H-bonding. This complex was further strengthened by hydrophobic interactions involving Asp334, Thr515, Ile569, Asp570, Met470, Asp566, Ile467, Pro471, Lys573, and His332 Within the complex (Fig. 7, Table 4).

Table 3. Topology parameters of essential compounds and targets in the network.

S. No.	Gene	Betweenness centrality	Degree	Compound	Betweenness centrality	Degree
1.	STAT3	0.0	1	Terpeniol	16819.188	99.0
2.	MAPK14	814.2	3.0	Limonene	12811.092	91.0
3.	MAPK1	0.0	1	p-menth- 8 ol	23767.615	95.1
4.	ESR1	9.41	3.0	Linalyl anthranilate	20592.5	85.0
5.	PTGS2	72.0	2.0	Myrecene	2310.4	26.0
6.	MAPK3	1.35	2.0	Beta-pinene	557.1	20.0
7.	EGFR	125	2.0			
8.	MAPK8	0.0	1			
9.	PPARG	1.35	2.0			
10.	PLA2G4A	0.0	1.0			

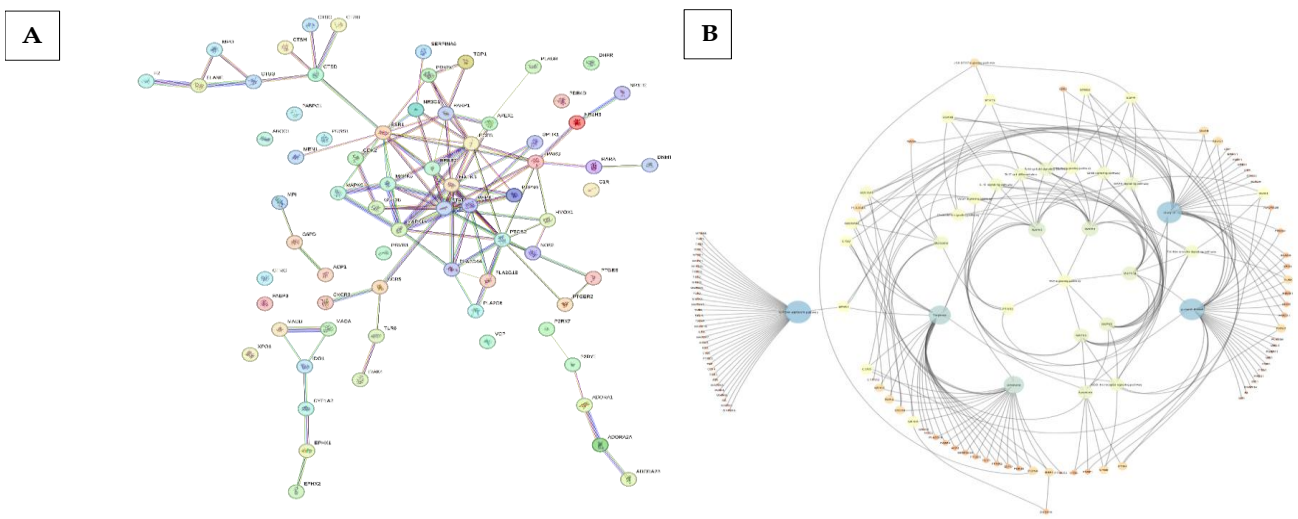

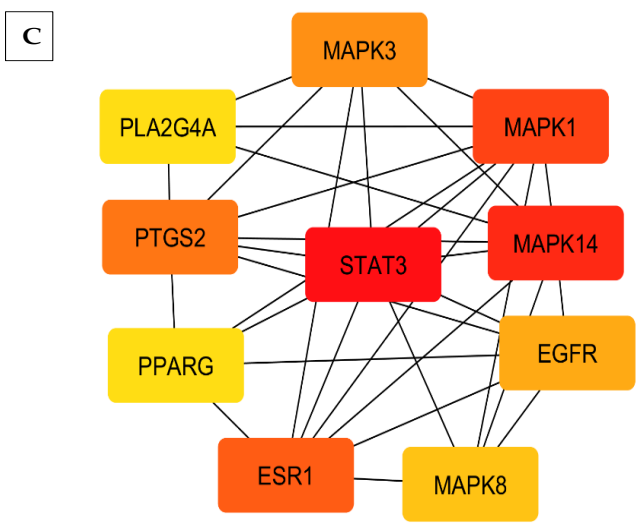

Rank	Name	Score
1	STAT3	168
2	MAPK14	132
3	MAPK1	124
4	ESR1	120
5	PTGS2	94
6	MAPK3	82
7	EGFR	75
8	MAPK8	54
9	PPARG	32
10	PLA2G4A	32

Fig. 4. A detailed overview of network analysis using PPI network (A), cytoscape merged networks (B), and hub genes (C).

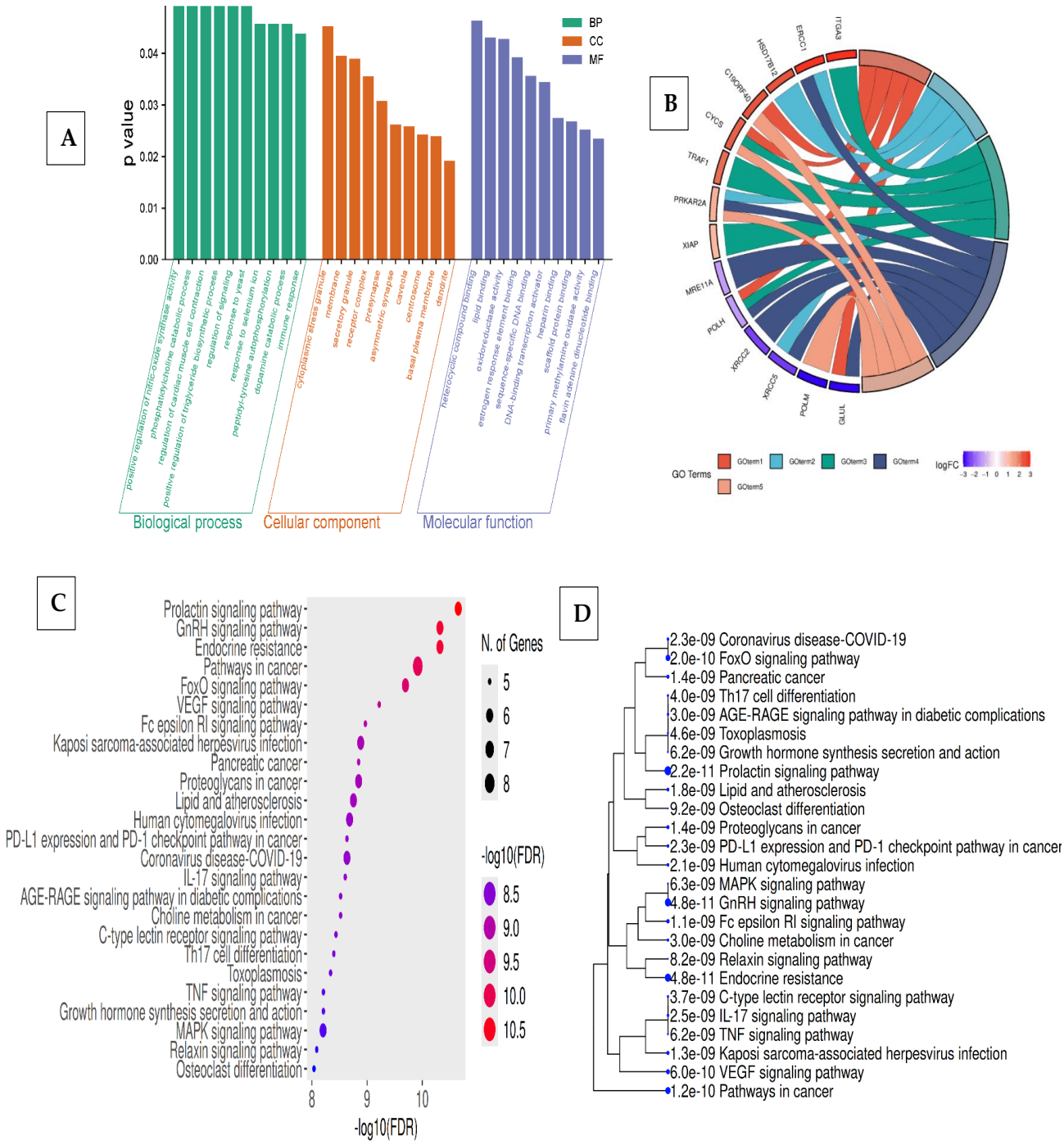

Fig. 5. GO Enrichment analyses of Top 10 biological processes, molecular functions, and Cellular components (A), circular diagram (B), KEGG enrichment result (C), and Correlation analysis (D).

Table 4. Molecular docking and interaction of analysed compounds.

S.No.	Target	PDB Id	Affinity kcal/mol	H bonding/Others
			Limonene	
1.	STAT3	1BG1	-5.8	**No**/ Leu103, Ile86, Cys166, Leu75, Lys54, Ala52, Val39, Ile84, Thr105
2.	MAPK14	7BDO	-6.5	**No**/ Val30, Phe169, Tyr35, Leu108, Val38, Met109, Ala51, Lys53, Thr106
3.	MAPK1	1PME	-4.6	**No**/ Ile569, Asp570, Asp566, Pro471, Met470, ArG335, Thr515, Asp334
			***p*-menth-8-en-ol-acetate**	
1.	STAT3	1BG1	-6.4	**Asp 167**/Cys166, Ile84, Ile31, Met108, Leu156, Ala52, Val 39, Leu107, Thr105, His106, Leu103, Lys54, Phe168, Leu75, Glu71
2.	MAPK14	7BDO	-5.2	**Asn82**/Tyr311, Phe129, Tyr132, Asp316, Glu81, Arg136, Gln133,
3.	MAPK1	1PME	-5.8	**Arg335**/ Asp334, Thr515, Ile569, Asp570, Met470, Asp566, Ile467, Pro471, Lys573, His332

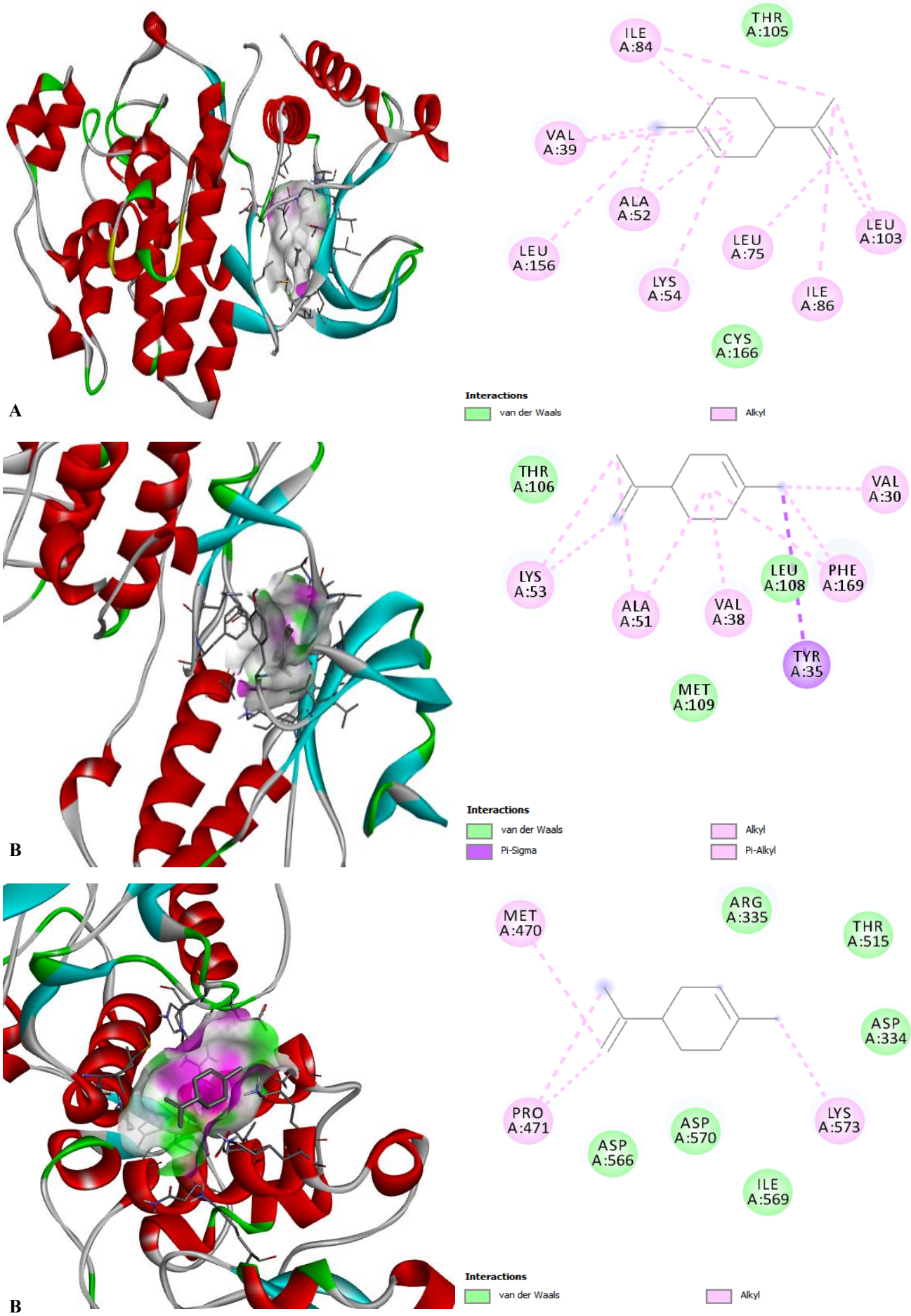

Fig. 6. Molecular docking and interaction analysis of Limonene with MAPK1 (A), MAPK14 (B), and STAT3 (C).

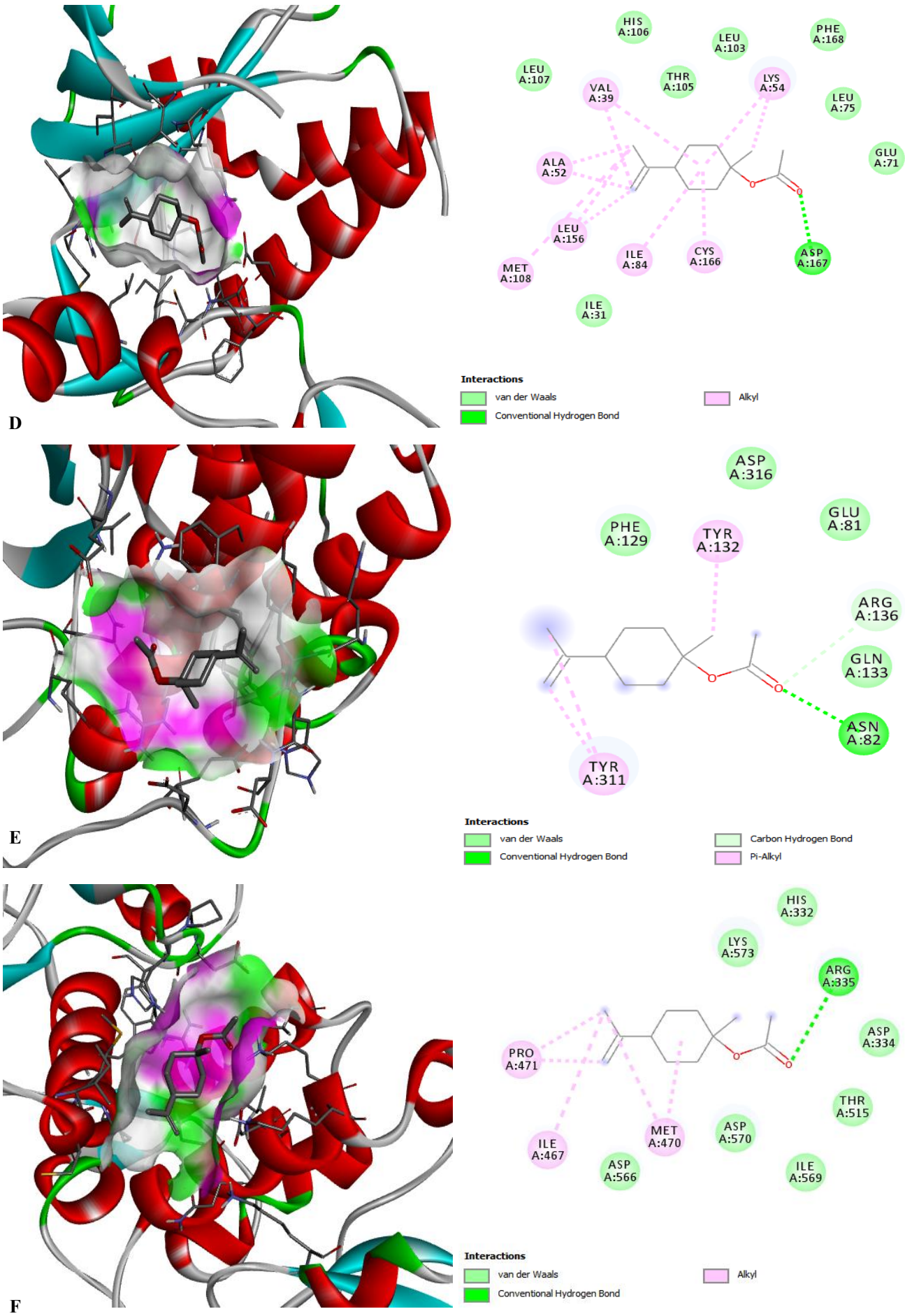

Fig. 7. Molecular docking and interaction analysis of *p*-menth-8-en-ol-acetate with MAPK1 (D), MAPK14 (E), and STAT3 (F).

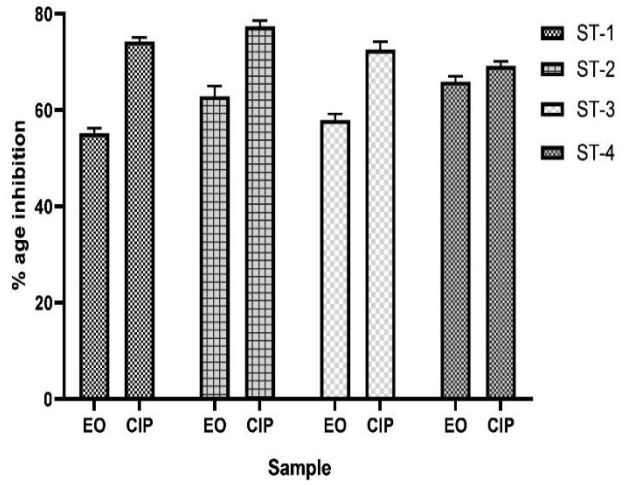

Fig. 8. Antibiofilm potential of all EO against *S. aureus* @2%(*v/v)*.

Antioxidant assays: The antioxidant profiling of EO was performed using FRAP, DPPH, and H_2O_2 assays. Here, the results revealed that EO responded well to all antioxidant mechanisms using diverse concentrations ranging from 2-10%(v/v). In the DPPH assay, radical scavenging was dose-dependent, with an IC50 range of 12.4-48.2 **µg/mL**. Similarly, in the **H_2O_2** assay, **the** highest inhibition was observed with EO-3 (78±1.6), followed by EO-2 (64±2.4) and E_1 (52±1.2). Finally, in the FRAP assay, the scavenging order was EO-3 > EO-2 > EO-1 (Table 5).

Antimicrobial screening (MICs): The *EO* was investigated against isolated strains (ST-1 -ST-4), and a moderate inhibition was observed against all analyzed strains (Table 6). Among the tested strains, significant activity was observed against ST-2 (MIC range 2.6-21.3 µg/mL v/v), followed by ST-1 (MIC range 10.6-21.3 µg/mL v/v). Likewise, in standard strains (ATCC), the MIC range was 1.3-10.4 µg/mL *v/v.* (Table 6).

Antibiofilm and time kill kinetics: Based on preliminary results, the sample EO-1 (EO-2%) was further processed for antibiofilm and time-kill kinetic studies. Among all, significant inhibition of biofilm produced by ST-2 was observed (77.4% ±1.4), followed by ST-1 (74.2±2.2) and ST-3 (72.6±1.6) (Fig. 8). The time-kill kinetics revealed promising results in strains ST-1 and ST-2, where biofilm suppression was observed till 18 hrs. In cases of ST-3 and ST-4, inhibition was observed for up to 8 hours, followed by a slight elevation in overall microbial count. However, overall, the EO inhibition levels against these two strains were comparable to those against ST-1 and ST-2. It was thus evident from this kinetic investigation that EO was effective against the analyzed strains at the tested concentration (2% v/v) (Fig. 9).

Table 5. Antioxidant profile of tested compounds.

Sample code	% Age	H_2O_2 % Inhibition	FRAP (µg)[2]	DPPH (IC_{50} µg/mL)
EO-1	EO-2%	52±1.2	224.5	48.2
EO-2	EO-5%	64±2.4	280.1	28.1
EO-3	EO-10%	78±1.6	306.4	12.4
STD	Standard[1]	76.2±2.2	-	6.4

[1]Ascorbic acid; [2]ascorbic acid equivalents, *

Table 6. Determination of antimicrobial activity (MIC % v/v) against isolated standard strains.

S.code	Sample	ST-1	ST-2	ST-3	ST-4	ST-RS
EO-1	EO-2%	21.3	5.3	10.2	5.3	10.4
EO-2	EO-5%	10.6	2.6	21.3	64	4.6
EO-3	EO-10%	21.3	21.3	10.6	21.3	1.3
	Standard drug	0.16	0.04	0.08	0.33	0.04

ST-RS *Staphylococcus aureus;* Reference strain; STD; ciprofloxacin

Discussion

A comprehensive phytochemical analysis of EO using GC–MS revealed the presence of several terpenoids, including limonene (61.2%) as the predominant constituent, followed by *p*-menth-8-en-ol acetate (14.1%), α-terpinene (10.2%), linalyl anthranilate (9.2%), myrcene (6.4%), and β-pinene (2.03%). This dominance of monoterpenes, especially limonene, aligns with prior reports that had confirmed *C. limon* EO as being rich in oxygenated and hydrocarbon monoterpenes, which were principally responsible for its biological activities (Bhattacharyya *et al*., 2024). However, differences in percentages of various constituents can be ascribed to maturity stage, geographical origin, and extraction conditions (Pham-Khanh & Nguyen, 2022).

It had also been reported earlier in the literature that a high proportion of limonene was acknowledged to confer strong antimicrobial, antioxidant, and anti-inflammatory properties. These activities may result from disrupting bacterial membranes and enhancing reactive oxygen species scavenging (Riaz *et al*., 2023). Moreover, oxygenated terpenes such as linalool and α-terpineol enhanced EO solubility and synergized antimicrobial efficacy (Hamdi *et al*., 2023).

The network pharmacology analysis identified 71 common targets between EO compounds and *Staphylococcus aureus pneumoniae*-associated genes. Hub genes, including STAT3, MAPK14, MAPK1, ESR1, and PTGS2, were highly interconnected, confirming that C. limon EO modulates inflammatory and stress-response pathways. These pathways have been implicated in bacterial virulence regulation and immune modulation (Pu *et al*., 2025).

The MAPK and IL-17 signaling pathways identified in the KEGG enrichment were key mediators of host-pathogen interactions. Limonene and related terpenes are likely to inhibit bacterial colonization by modulating MAPK-related phosphorylation cascades (Fikry *et al*., 2025). These findings validated preceding investigations using integrated GC–MS and network pharmacology approaches for *Citrus* oils, accenting their multitarget anti-infective potential (Tian *et al*., 2025).

The hub genes identified were processed for docking simulations, which revealed significant interactions between limonene and p-menth-8-en-ol acetate and key targets, including STAT3, MAPK14, and MAPK1, with associated binding affinities. The *P*-menth-8-en-ol acetate formed stable hydrogen bonds with Asp167 (STAT3) and Arg335 (MAPK1), suggesting a more substantial inhibitory potential than limonene. Such binding energies were consistent with previous reports showing that Citrus terpenoids exhibited favorable interactions with bacterial and inflammatory proteins (Saleem *et al*., 2023). These outcomes suggest that *C. limon* EO components exhibit

antibacterial and anti-inflammatory effects by interfering with MAPK-mediated signaling, supporting the predictive network pharmacology data.

For experimental validation of results, the EO was first analyzed for antioxidant potential and showed concentration-dependent activity across DPPH, FRAP, and H_2O_2 assays, with the strongest performance at 10% (v/v) (IC_{50} = 12.4 µg/mL). This activity can be mainly attributed to monoterpenes' ability to donate hydrogen atoms and scavenge free radicals (Riaz *et al*., 2023). Comparable IC_{50} values were observed in *C. medica* and *C. reticulata* oils, reinforcing the significant antioxidant power of limonene- and α-terpinene-rich oils (Khanh Nguyen *et al*., 2024). The hydrogen peroxide and FRAP data also confirmed redox modulation and potential membrane-protective effects, which were key to mitigating oxidative stress in bacterial infections.

In the antimicrobial assays, EO showed moderate to vigorous antibacterial activity, with MIC values of 1.3–21.3 µg/mL, and was most potent against *S. aureus* (ST-2). Similar antibacterial potency against Gram-positive bacteria had previously been linked to the lipophilic nature of limonene and myrcene, which increased membrane permeability and induced leakage of cellular contents (Kaspute *et al*., 2025). The EO also exhibited noteworthy antibiofilm activity, inhibiting biofilm formation by up to 77% at 2% (*v/v*). This antibiofilm potential can be best described by interference in quorum sensing and suppression of extracellular polymeric substance production. These findings were consistent with observations in *Anethum graveolens* and *Citrus paradisi* Eos (Hamdi *et al*., 2023). Finally, Time-kill kinetics showed constant bacterial suppression up to 18 h, consistent with reports that EO components may infiltrate biofilm layers and maintain extended bactericidal activity (Rossi *et al*., 2022). The demonstrated antioxidant, antibacterial, and antibiofilm properties also carry significant implications for food science. Citrus essential oils were emerging as natural preservative agents capable of replacing synthetic additives in functional foods due to their strong radical-scavenging capacity and ability to inhibit microbial growth in food matrices. The potent antibiofilm action observed against *S. aureus* suggests practical applications in preventing biofilm formation on food processing equipment, thereby reducing contamination risks. Given the high limonene content and the GRAS status of citrus oils, the Singhar variety essential oil may be incorporated into active food packaging, edible coatings, or nutraceutical formulations to enhance food safety and extend shelf-life.

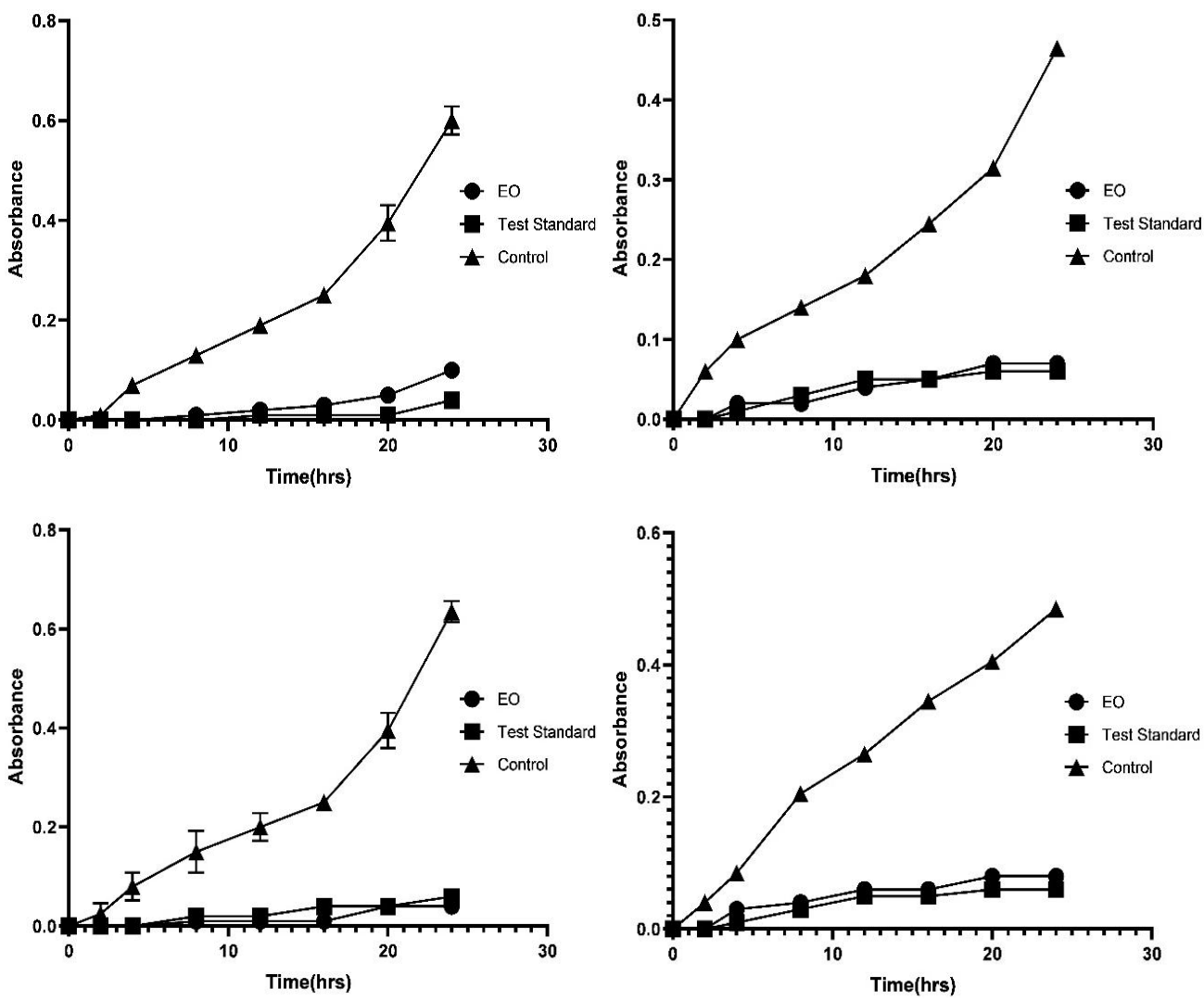

Fig. 9. Time kill kinetics of S. aureus strains ST-1 (A), ST-2(B), ST-3 (C) and ST-4 (D) against *C-limon* EO @2%(*v/v)*.

Conclusion

This study includes the extraction of essential oil from the indigenous *Citrus limon* "Singhar" variety and analysis against methicillin-resistant *Staphylococcus aureus* biofilms. By using an integrated in silico and in vitro approach, we discovered that the bioactivity of this EO is principally driven by its rich monoterpene content, especially limonene and p-menth-8-en-ol acetate. Network pharmacology and molecular docking analyses indicated strong interactions with key bacterial and inflammatory targets, including STAT3, MAPK14, and MAPK1, implicating mechanisms that disrupt host-pathogen signaling pathways, including the MAPK and IL-17 cascades. Antioxidant assays confirmed the EO's potent free radical scavenging ability. At the same time, antibacterial and antibiofilm studies validated its efficacy across multiple clinical and reference strains, demonstrating notable biofilm inhibition (up to 77.4%) and sustained bactericidal activity for 18 hours. Collectively, the chemical, computational, and biological data confirm that the Singhar *Citrus limon* essential oil possesses vigorous multifunctional activity suitable for both therapeutic and food-related applications. Given its food-grade origin and high monoterpene content, this essential oil is a promising natural preservative that can enhance food safety through antioxidant, antibacterial, and antibiofilm mechanisms. These findings highlight its potential incorporation into nutraceuticals, functional foods, and natural food preservation systems. Future work should evaluate its stability in food matrices, its sensory impact, and its synergistic effects with conventional preservation methods to support its development for practical food applications.

Acknowledgements

This research was supported by the "Regional Innovation System & Education (RISE)" through the Seoul RISE Center, funded by the Ministry of Education (MOE) and the Seoul Metropolitan Government (2025-RISE-01-035-05). This work was also supported by the National Research Foundation of Korea (NRF) grant funded by the Korean government (MSIT) (No. RS- 2023-00252468). Additionally, this work was supported by the Hongik University new faculty research support fund.

Conflicts of Interest: The authors declare no conflict of interest.

Authors Contribution: A.A., A.A., S.A. and W.Z. performed the experimental work, data analysis and writing and editing the final draft. M.L. and Y.G. contributed to computational analysis, interpretation of results and writing the draft. Y.S.H. conceptualized the study, supervised the research, and finalized the manuscript. All authors read and approved the final manuscript.

References

Al-Khayri, J.M., A. Banadka, M. Nandhini, P. Nagella, M.Q. Al-Mssallem and F.M. Alessa. 2023. Essential oil from: A review on its phytochemistry and biological activity. *Molecules, 28*(2): 696. doi: ARTN 69610.3390/molecules28020696

Amanullah, F.U. Rehman, U. Aiman, S.O. Rab, S. Awais, R. Baloch and A. Amin. 2025. Synthesis of new nicotintaldehyde derivatives via Pd(0) catalyzed suzuki coupling with structural characterization and co-combined computational-experimental evaluation against oral pathogens. *Scientific Reports,* 15(1): 22205. doi:10.1038/s41598-025-05156-0

Azad, N. and C. Chhatria. 2025. Antioxidant activity of hydroethanolic extracts of *Asteracantha longifolia* and *Moringa oleifera* using DPPH, nitric oxide, hydrogen peroxide and frap model. *Asian Journal of Biology,* 21(7): 120-129.

Bhattacharyya, S., S.D. Sarma, P. Dutta, T. Begum, M. Lal, K. Perveen and N.A. Bukhari. 2024. Insights into *Citrus limon* (L.) Osbeck peel essential oil from NE India: A study of its pharmacological properties and chemical composition. *Journal of Essential Oil Bearing Plants,* 27(5): 1362-1376. doi:10.1080/0972060X.2024.2411408

de Sousa, D., R.O.S. Damasceno, R. Amorati, H.A. Elshabrawy, R.D. de Castro, D.P. Bezerra and T.C. Lima. 2023. Essential oils: Chemistry and pharmacological activities. *Biomolecules,* 13(7): 1144.

Fikry, E., R. Orfali, S. Perveen, S. Ghaffar, A.M. El-Shafae, M.M. El-Domiaty and N. Tawfeek. 2025. Chemical composition and anti-lung cancer activities of *Melaleuca quinquenervia* leaf essential oil: Integrating Gas Chromatography–Mass Spectrometry (GC/MS) Profiling, Network Pharmacology, and Molecular Docking. *Pharmaceuticals,* 18(6): 771.

Gölükcü, M., B. Bozova, H. Tokgöz, D.Y. Turgut, O. Çınar, E. Turgutoglu and A.M. Giuffrè. 2024. Effects of cultivar, harvesting time and isolation techniques on the essential oil compositions of some lemon cultivars. *AIMS Agriculture and Food,* 9(3): 904-920. doi:10.3934/agrfood.2024049

Guerra, M.E.S., G. Destro, B. Vieira, A.S. Lima, L.F.C. Ferraz, A.P. Hakansson and T.R. Converso. 2022. Biofilms and their role in disease pathogenesis. *Frontiers in Cellular and Infection Microbiology,* 12: 877995. doi:ARTN 87799510.3389/fcimb.2022.877995

Hamdi, A., M. Horchani, H.B. Jannet, M. Snoussi, E. Noumi, N. Bouali and H. Edziri. 2023. *In vitro* screening of antimicrobial and anti-coagulant activities, ADME profiling, and molecular docking study of *Citrus limon* L. and *Citrus paradisi* L. cold-pressed volatile oils. *Pharmaceuticals,* 16(12): 1669.

Kačániová, M., N. Čmiková, N.L. Vukovic, A. Verešová, A. Bianchi, S. Garzoli and M.D. Vukic. 2024. *Citrus limon* essential oil: Chemical composition and selected biological properties focusing on the antimicrobial (*In vitro*, *In situ*), antibiofilm, insecticidal activity and preservative effect against *Salmonella enterica* inoculated in carrot. *Plants,* 13(4): 524. doi:10.3390/plants13040524

Kaspute, G., T. Ivaskiene, A. Ramanavicius, S. Ramanavicius and U. Prentice. 2025. Terpenes and essential oils in pharmaceutics: applications as therapeutic agents and penetration enhancers with advanced delivery systems for improved stability and bioavailability. *Pharmaceutics,* 17(6): 793.

Khanh Nguyen, N.P., J.-H. Kwon, M.-K. Kim, K.N. Tran, L.T. Huong Nguyen and I.-J. Yang. 2024. Antidepressant and anxiolytic potential of *Citrus reticulata* Blanco essential oil: A network pharmacology and animal model study. *Frontiers in Pharmacology,* Volume 15-2024.

Namivandi-Zangeneh, R., Y. Yang, S. Xu, E.H.H. Wong and C. Boyer. 2019. Antibiofilm platform based on the combination of antimicrobial polymers and essential oils. *Biomacromolecules,* 21(1): 262-272. doi:10.1021/acs.biomac.9b01278

Noumi, E., I. Ahmad, M. Adnan, A. Merghni, H. Patel, N. Haddaji and V. De Feo. 2023. GC/MS profiling, antibacterial, anti-quorum sensing, and antibiofilm properties of *L. essential* oil: Molecular docking study and *In-silico* ADME profiling. *Plants-Basel,* 12(10): 1997. doi:ARTN 199710.3390/plants12101997

Pal, M., T. Rebuma, T. Regassa and R. Zende. 2024. Methicillin-resistant *Staphylococcus aureus* (Mrsa) remains a major threat to public health. *American Journal of Public Health Research,* 12(3): 48-53.

Paw, M., T. Begum, R. Gogoi, S.K. Pandey and M. Lal. 2020. Chemical composition of *L. burmf* peel essential oil from north east India. *Journal of Essential Oil Bearing Plants,* 23(2): 337-344. doi:10.1080/0972060x.2020.1757514

Pham-Khanh, N.-H. and T.-T. Nguyen. 2022. Gas chromatography-mass spectrometry, feature-based molecular networking and biological activities against *Solenopsis invicta* of *Citrus peel* essential oils from Vietnam. *Agriculture and Natural Resources,* 56(4): 805-814.

Pickens, C.I. and R.G. Wunderink. 2022. *Methicillin-resistant Staphylococcus aureus hospital-acquired pneumonia/ ventilator-associated pneumonia*.

Pu, J., J. Cui, H. Yang, J. Cao, S. Xiao and G. Cheng. 2025. The anti-inflammatory effects and molecular mechanism of citri reticulatae pericarpium essential oil: A combined GC-MS and network pharmacology study. *Foods,* 14(9): 1455.

Rossi, C., C. Chaves-López, A. Serio, M. Casaccia, F. Maggio and A. Paparella. 2022. Effectiveness and mechanisms of essential oils for biofilm control on food-contact surfaces: An updated review. *Critical Reviews in Food Science and Nutrition,* 62(8): 2172-2191.

Saleem, M., A.I. Durani, A. Asari, M. Ahmed, M. Ahmad, N. Yousaf and M. Muddassar. 2023. Investigation of antioxidant and antibacterial effects of citrus fruits peels extracts using different extracting agents: Phytochemical analysis with *In silico* studies. *Heliyon,* 9(4). doi:10.1016/j.heliyon.2023.e15433

Sharifi-Rad, J., A. Sureda, G. Tenore, M. Daglia, M. Sharifi-Rad, M. Valussi and M. Iriti. 2017. Biological activities of essential oils: From plant chemoecology to traditional healing systems. *Molecules,* 22(1): 70. doi:10.3390/molecules22010070

Subramenium, G.A., K. Vijayakumar and S.K. Pandian. 2015. Limonene inhibits streptococcal biofilm formation by targeting surface-associated virulence factors. *Journal of Medical Microbiology*, 64, 879-890. doi:10.1099/jmm.0.000105

Tang, C.L., J.L. Chen, L.X. Zhang, R.F. Zhang, S.C. Zhang, S.X. Ye and D.P. Yang. 2020. Exploring the antibacterial mechanism of essential oils by membrane permeability, apoptosis and biofilm formation combination with proteomics analysis against methicillin-resistant. *International Journal of Medical Microbiology,* 310(5): 151435. doi:ARTN 15143510.1016/j.ijmm.2020.151435

Tian, L., P.Y. Zom and C. Ma. 2025. Based on network pharmacology, molecular docking, and validation experiments to investigate the active components and mechanisms of action of Tibetan Medog County Citrus medica L.: In antioxidant activity. *Medicine,* 104(42): e45036. doi:10.1097/md.0000000000045036

Trott, O. and A.J. Olson. 2010. AutoDock Vina: improving the speed and accuracy of docking with a new scoring function, efficient optimization, and multithreading. *Journal of Computational Chemistry,* 31(2): 455-461.

Tullio, V., J. Roana, L. Cavallo and N. Mandras. 2023. Immune defences: A view from the side of the essential oils. *Molecules,* 28(1): 435. doi:ARTN 43510.3390/ molecules28010435

Wang, X., S. Guo, J. Chen, R. Cheng, F. Zhou, L. Huang and C. Li. 2025. Integrated network pharmacology and molecular docking combined with metabolomics to identify the pharmacological mechanism of Jiedu Huoxue decoction against cisplatin-induced acute kidney injury. *Journal of Ethnopharmacology*, 120088.

Wang, X., M. Liu, C. Yu, J. Li and X. Zhou. 2023. Biofilm formation: Mechanistic insights and therapeutic targets. *Molecular biomedicine,* 4(1): 49.